Elastographic Imaging of Strain Distribution in the Anterior Cruciate Ligament and at the Ligament–Bone Insertions

Jeffrey P. Spalazzi,[1] Jason Gallina,[1,4] Simon D. Fung-Kee-Fung,[3] Elisa E. Konofagou,[3] Helen H. Lu[1,2]

[1]Biomaterials and Interface Tissue Engineering Laboratory, Department of Biomedical Engineering, Columbia University, 351 Engineering Terrace Building, MC 8904, 1210 Amsterdam Avenue, New York, New York 10027

[2]College of Dental Medicine, Columbia University, New York, NY 10032

[3]Ultrasound and Elasticity Imaging Laboratory, Department of Biomedical Engineering, Columbia University, New York, NY 10027

[4]St. Luke's/Roosevelt Hospital Center, Department of Orthopaedic Surgery, New York, NY 10019

Received 6 January 2006; accepted 13 May 2006

Published online 9 August 2006 in Wiley InterScience (www.interscience.wiley.com). DOI 10.1002/jor.20260

ABSTRACT: The anterior cruciate ligament (ACL) functions as a mechanical stabilizer in the tibiofemoral joint, and is the most commonly injured knee ligament. To improve the clinical outcome of tendon grafts used for ACL reconstructions, our long-term goal is to promote graft–bone integration via the regeneration of the native ligament–bone interface. An understanding of strain distribution at this interface is crucial for functional scaffold design and clinical evaluation. Experimental determination, however, has been difficult due to the small length scale of the insertion sites. This study utilizes ultrasound elastography to characterize the response of the ACL and ACL–bone interface under tension. Specifically, bovine tibiofemoral joints were mounted on a material testing system and loaded in tension while radiofrequency (RF) data were acquired at 5 MHz. Axial strain elastograms between RF frames and a reference frame were generated using crosscorrelation and recorrelation techniques. Elastographic analyses revealed that when the joint was loaded in tension, complex strains with both compressive and tensile components occurred at the tibial insertion, with higher strains found at the insertion sites. In addition, the displacement was greatest at the ACL proper and decreased in value gradually from ligament to bone, likely a reflection of the matrix organization at the ligament–bone interface. Our results indicate that elastography is a novel method that can be readily used to characterize the mechanical properties of the ACL and its insertions into bone. © 2006 Orthopaedic Research Society. Published by Wiley Periodicals, Inc. J Orthop Res 24:2001–2010, 2006

Keywords: anterior cruciate ligament; elastography; insertions; strain distribution; ultrasound

INTRODUCTION

The anterior cruciate ligament (ACL) serves as a mechanical stabilizer for the tibiofemoral joint and is the most frequently injured knee ligament, with approximately 100,000 reconstructions performed each year in the United States.[1–4] Due to the poor healing potential of the ACL,[5] surgical intervention is required following ligament injury. Two types of autografts commonly utilized to replace the ACL include the bone–patellar tendon–bone graft and the hamstring tendon (HT) graft. The HT has become the most commonly utilized graft type for ACL reconstruction due to its relatively low donor site morbidity.[6,7] However, this soft tissue-based graft is mechanically anchored to bone, and the lack of biological fixation compromises its long-term clinical outcome.

The native ACL connects to bone through a direct insertion consisting of a linear transition from ligament to fibrocartilage to bone.[8] The fibrocartilage zone is further divided into nonmineralized and mineralized regions.[9] Due to the presence of more than one type of tissue, the ACL–bone interface is expected to vary in cellular, chemical, and mechanical properties. This controlled matrix heterogeneity is believed to permit a gradual transition of mechanical load between soft tissue and bone, and in turn, minimizes the formation of stress concentrations.[10] This insertion site, however, is not reestablished after tendon graft-based ACL reconstruction. Without a stable interface, the fixation site of HT grafts to bone becomes the weak link in the reconstructed graft

Correspondence to: Helen H. Lu (Telephone: 212-854-4071; Fax: 212-854-8725; E-mail: hl2052@columbia.edu)

and the leading cause of graft failure and subsequent revision surgery.[11–16] Our long-term goal is to promote graft–bone integration by tissue engineering a functional soft tissue–bone interface. Our success depends on understanding the mechanical properties of the ACL and the ACL–bone interface, which are important in biomaterial selection and interface regeneration via tissue engineering methods. Elucidating the structure–function relationship at the insertions is critical for the design of new graft fixation devices capable of biological fixation through the reestablishment of the native soft tissue–bone interface.[17–20]

Classical mechanical testing techniques combined with optical tracking of stain lines, pins, and fiducial markers have provided a thorough understanding of the mechanical response of the femur–ACL–tibia complex and ACL midsubstance.[21–31] When Butler et al.[31] evaluated the strain distribution within the ACL by performing failure tests of human ACL subbundles, a spatial variation in strain was measured along the length of the ACL, with the greatest strain found at the insertion sites. The type, magnitude, and distribution of strain at the ACL–bone junction have not been reported. Experimental determination of the mechanical properties of the ACL insertions has been limited due to the relatively small length scale of the insertion sites, which span approximately 700– 800 μm in neonatal bovine and even smaller lengths in humans. Several finite element (FE) models have been used to predict the mechanical behavior of the ACL and insertions.[32–36] However, due to spatial resolution and other experimental limitations of traditional mechanical testing techniques, primarily the inability to distinguish the response of subsurface microscale ACL insertion transitional tissues from the entire ligament complex, no experimental validation of FE models has been possible.

This study investigates the mechanical response of the insertion sites using the method of ultrasound elastography. Elastography or elasticity imaging has been used to map mechanical responses and calculate material properties by comparing ultrasound or MR images acquired before and after mechanical loading. This technique, developed in the early 1990s as an alternative tool for early tumor detection and diagnosis based on the principle of palpation,[37,38] has been extensively validated and utilized in intravascular and cardiovascular applications in vivo,[39,40] as well as in the guidance of thermal therapy procedures.[41] Elastography has been used to determine both elastic and mechanical properties of tissues.[38] Ultrasound elastography in particular has been used to image the mechanical properties of articular cartilage under compression.[42–45]

The objectives of this study were to use ultrasound elastography to characterize the mechanical response of ACL insertions and to image strain distributions in the ACL proper and at the ACL–bone insertions. Elastography represents a novel and reliable technique suitable for evaluation of the ACL–bone interface as it permits the characterization of a relatively small region consisting of complex tissue types. In this method, the ultrasound transducer scans the region of interest while an external load is applied to induce strain inside the tissue. Speckle tracking techniques are then employed to analyze the acquired radiofrequency (RF) ultrasonic data before and after incremental loading and to estimate the resulting strain and strain distributions.[46] Time-dependent changes in mechanical properties can be monitored in real time and quantified. In this study, the mechanical response of the ACL and ACL–bone insertion region under applied tensile loading were imaged. The incremental displacement and strain distributions at the ligament and its insertions were determined using a bovine model.

MATERIALS AND METHODS

Neonatal bovine tibiofemoral joints were obtained from an abattoir. After removal of surrounding muscle and adipose tissue, the joint capsule was exposed. Fascia lata and connective tissue were removed from the capsule with the ACL and posterior cruciate ligament (PCL) left intact. During all preparation procedures, the ACL and surrounding tissues were kept hydrated with physiologic saline. The femur and tibia were cut approximately 12 cm from the joint. The periosteum was removed and bone marrow was extracted from the intramedullary cavity to improve cement fixation of the joint. Subsequently, the tibia and femur were secured with custom anchors and cemented to prevent slippage during testing. The joint was mounted on a uniaxial material testing system (MTS 858 Bionix Testing System; MTS, Eden Prairie, MN) fitted with a custom cylindrical polycarbonate tank. Before loading, the PCL was severed and the medial femoral condyle was removed to improve line-of-sight access to the ACL and insertions within the field of view of the ultrasound image (Fig. 1a).

Tensile testing was performed with the femur–ACL–tibia complex ($n = 3$) set in a tibial alignment following the methods of Woo et al.[29] with modifications to accommodate ultrasound imaging. Briefly, the femur and tibia were aligned along the tensile axis with 0° of knee flexion, and the sample was submerged in degassed physiologic saline. In addition to preventing tissue dehydration, the saline provided a medium for

 DOI 10.1002/jor

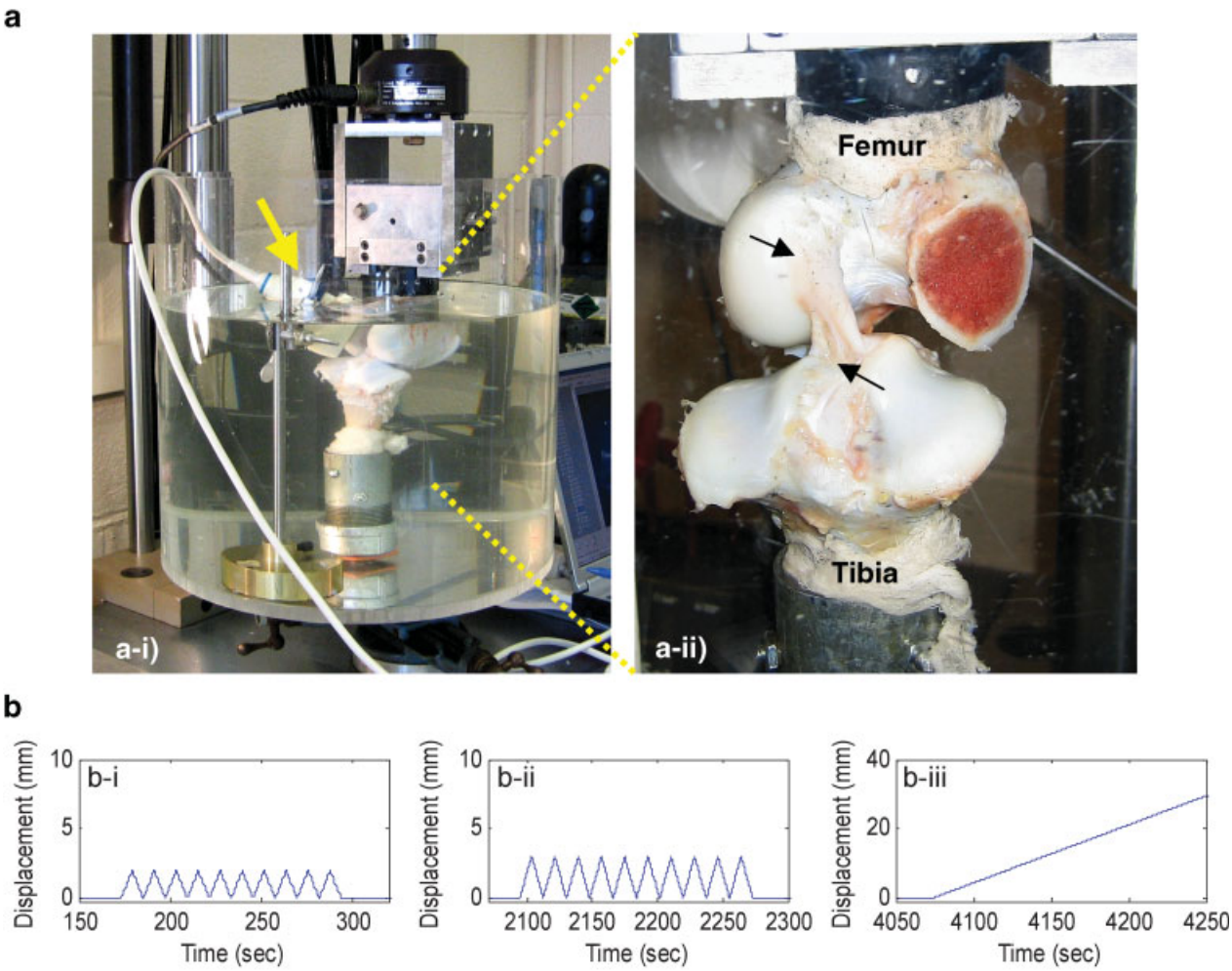

Figure 1. Mechanical testing of the bovine patellofemoral joints and image acquisition using an ultrasound transducer. (a-i) The joint was loaded in the MTS modified with a customized saline tank, and the ultrasound transducer (yellow arrow) was mounted inside the tank. The ligament and the ligament-to-bone insertions were scanned posteriorly. (a-ii) Posterior view of the joint (ACL insertion sites labeled with black arrows) mounted in a tibial orientation and with 0° flexion. (b) Ultrasound RF data was acquired while the joint was loaded in tension. Three loading regimens were applied: (i) 0–2 mm at a rate of 20 mm/min, (ii) 0–3 mm at a rate of 20 mm/min, (iii) load to failure at a rate of 10 mm/min.

ultrasound propagation. A preload of 2 N was applied for 1 min, and the joint was preconditioned by cyclic loading (0–0.75 mm) for 10 cycles at 20 mm/min followed by a rest of 1 min. Three sequential loading regimens (Fig. 1b) were applied to each sample. First, the joint was cyclically loaded from 0 to 2 mm at 20 mm/min, with 0 mm set as the initial displacement during the preload. Small displacements were applied initially for speckle tracking to be optimal for elastographic analysis. Following a 30-min rest, the joint was cyclically loaded from 0 to 3 mm, with additional displacement applied during this testing regimen to ensure an elastographically detectable amount of deformation occurred across the insertions. Finally, after an additional 30-min rest, the joint was loaded to failure at 10 mm/min.[29,47–49]

During loading, an ultrasound scanner (Terason 2000; Teratech, Inc., Rockville, MD) was used to acquire RF data at 5 MHz via a linear array. The ultrasound transducer was mounted inside the saline tank and positioned to image the ACL and the femoral and tibial insertions. Sequences of RF data were acquired continuously during deformation at 54 frames/s for intervals of 3 s (128 RF lines, sampling frequency: 10 MHz).

The axial displacement between the reference and successive frames was estimated offline and imaged using crosscorrelation and recorrelation techniques with a window size of 3 mm and a window overlap of 80%.[38,44] Axial displacements (i.e., displacements occurring orthogonal to the face of the transducer and parallel to the direction of ultrasound pulse propagation) were

estimated for each RF frame with respect to the reference frame using a 1D crosscorrelation algorithm. In this algorithm, time-shifts between two backscattered RF signals were determined using crosscorrelation of small windowed segments over the entire 2D ultrasound image.[38] At high decorrelation noise, recorrelation techniques were employed.[44] Finally, the strain distribution was computed by differentiating the displacement map along the axial direction. For numerical differentiation, a least-squares regression method was used.[50] Displacement and strain were estimated relative to a reference ultrasound RF frame, which was captured before the application of tensile load, to obtain a temporal profile and map of the cumulative deformation at the ligament and the insertion.

RESULTS

In all specimens tested, the ACL, femoral insertion (FI), and tibial insertion (TI) of the ACL, and femoral or tibial bone were clearly identifiable on the ultrasound images (Fig. 2b) and in all subsequent displacement maps (Fig. 2c) and strain elastograms (Fig. 2d). Each tissue type exhibited a distinct ultrasound signature. This resulted in tissue-specific speckle patterns distinguishing ligament, articular cartilage, and subchondral bone (Fig. 2b). Differences between soft and hard tissue signatures were used to identify the ACL insertions into bone. Due to its high density, bone is strongly hypoechoic, resulting in specular reflection at the ligament–bone interface and poor ultrasound propagation within the tissue. Therefore, bone appears black on the B-mode ultrasound images (Fig. 2b). The ligament is more uniform, and therefore hyperechoic, enabling the tissue structure to be discernable on the B-mode images. Within the ACL, a narrow band of high strain in the middle and along the length of the ACL was observed and corresponded to a highly echogenic area on the B-mode images. This may reflect the

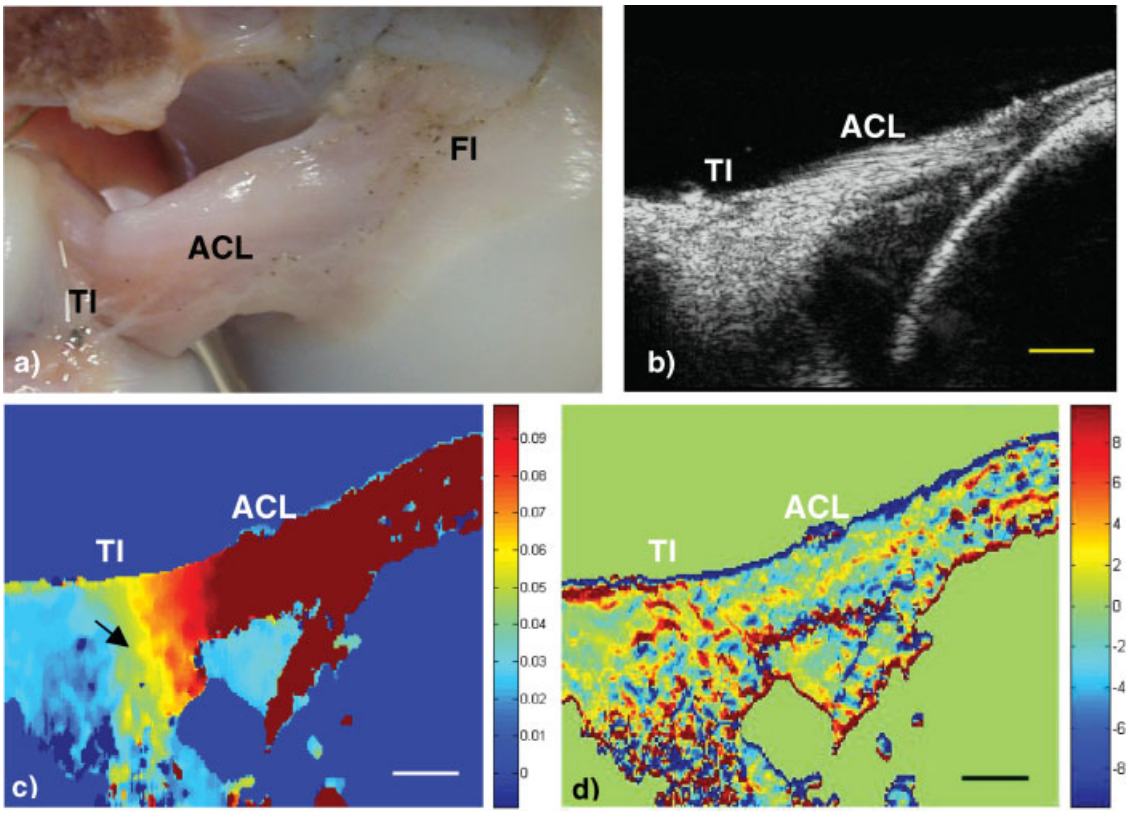

Figure 2. Elastographic analysis of the ACL and its insertions. (a) Posterior view of the scanned ACL and the tibial insertion (TI) and femoral insertion (FI) sites. (b) Ultrasound image of the ACL and tibial insertion. (c) Corresponding displacement map calculated from RF data, with blue to red, indicating small to large displacements (mm), respectively. (d) Corresponding elastogram with percent compressive strain indicated in blue and tensile strain in red. Negative values denote compressive strain. Note the complex strain distribution at the insertion sites with both compressive and tensile strain detected at the insertion. (scale bars = 5 mm).

 DOI 10.1002/jor

organization of the ACL, which consists of anteromedial and posterolateral bundles.[51,52]

After confirming the feasibility of imaging the ACL and insertions with ultrasound and establishing clear identification of the tissue regions, the localized mechanical behavior of the ACL and tibial insertion was determined using ultrasound elastography. Elastographic analysis yielded maps of cumulative deformation and strain in the ACL and its tibial insertion during tensile loading. The distribution of tissue deformation in the femur–ACL–tibia complex is shown in Figure 2c, with magnitudes of deformation represented from high (red) to low (blue). The displacement was found to be the highest (red in Fig. 2c) within the ACL proper and decreased in a gradual transition from ligament (red) to interface (orange) to the bone surface (blue). In addition, strain maps (Fig. 2d) revealed that the strain profile at the tibial insertion was highly complex. Both compressive and tensile strains were evident at the insertion site, indicated by the green–blue and yellow–red regions, respectively. A narrow blue region along the entire upper tissue–saline interface in the elastogram (Fig. 2d) is an artifact of the high acoustical impedance difference between the femur–ACL–tibia complex and saline, and should not be misinterpreted as compressive strain. Compressive strains (blue) found within the ACL proper were largely artifacts as the transducer was aligned with respect to the insertion (region of interest in this study) during loading.

The accumulation of deformation and strain throughout the entire femur–ACL–tibia complex is evident in Figure 3, which shows deformation (Fig. 3a) and strain (Fig. 3b) for a sequence of 16 frames with respect to a single reference frame. Although the deformation remained relatively constant in the bone region (blue) over time from frames 1–16 (0.1 mm total displacement) significant changes were found in the ACL proper, as shown by the increase in deformation reflected in the color change of the ACL region from blue to green, yellow, orange, and finally red in the ACL region (Fig. 3a). Pointwise temporal displacement and strain analysis of the deformation at the tibial insertion over time demonstrated that under applied tension, complex strain with both compressive (blue) and tensile (red) components were detected at the interface between ACL and bone. To confirm the existence of compressive strain in the insertion, further analysis was performed focused on a specific point on the elastogram at which the compressive strain could be clearly observed. These results are presented in Figure 4, which shows the displacement and strain response at a single point (chosen from Fig. 2c, arrow). This point corresponds to a 0.3×0.6-mm region within the tibial insertion that was clearly undergoing compressive strain, and a constant rate of deformation was observed, with a corresponding nonconstant evolution of compressive strain.

In the elastographic analysis method, displacement and strains are measured along the axis parallel to the direction of ultrasound beam propagation. This may introduce artifacts corresponding to the orientation of the transducer with respect to the femur–ACL–tibia complex. To ensure that our results were independent of the transducer orientation, an additional trial was performed with the transducer rotated such that its face was aligned with the principal axis of the ACL (Fig. 5). A gradual decrease in deformation was again observed across the insertion, with high deformation (green) imaged in the ACL proper, a lower magnitude of deformation detected in bone (dark red), and a transition from green to yellow, orange, and red observed at the interface between the ACL and bone (Fig. 5b). More importantly, compressive strain (blue regions, Fig. 5c) was again found at the interface when the joint was loaded in tension, and the artifact compressive strain in the ACL proper evident in Figure 5 was no longer present. Only tensile strains (red regions) were seen in the ACL proper. These results are consistent with those presented in Figure 2 and collectively demonstrate that when the joint was loaded in tension, both compressive and tensile strains were present at the interface between ligament and bone.

DISCUSSION

We have reported here the first experimental determination of the localized mechanical response of the ACL and its insertions using ultrasound elastography. Our objective was to evaluate the feasibility of utilizing this novel functional imaging technique to determine the mechanical response and strain distribution at the insertion sites. Under tensile loading, the strain distribution at the ACL–bone insertion was found to be highly complex, with both tensile and compressive components. In addition, the magnitude of deformation was highest in the ACL proper, with a gradual decrease across the ACL–bone transition, suggesting increasing tissue stiffness from ligament to bone.

Currently, no gold standard exists for determining strains at the insertion. The aforementioned

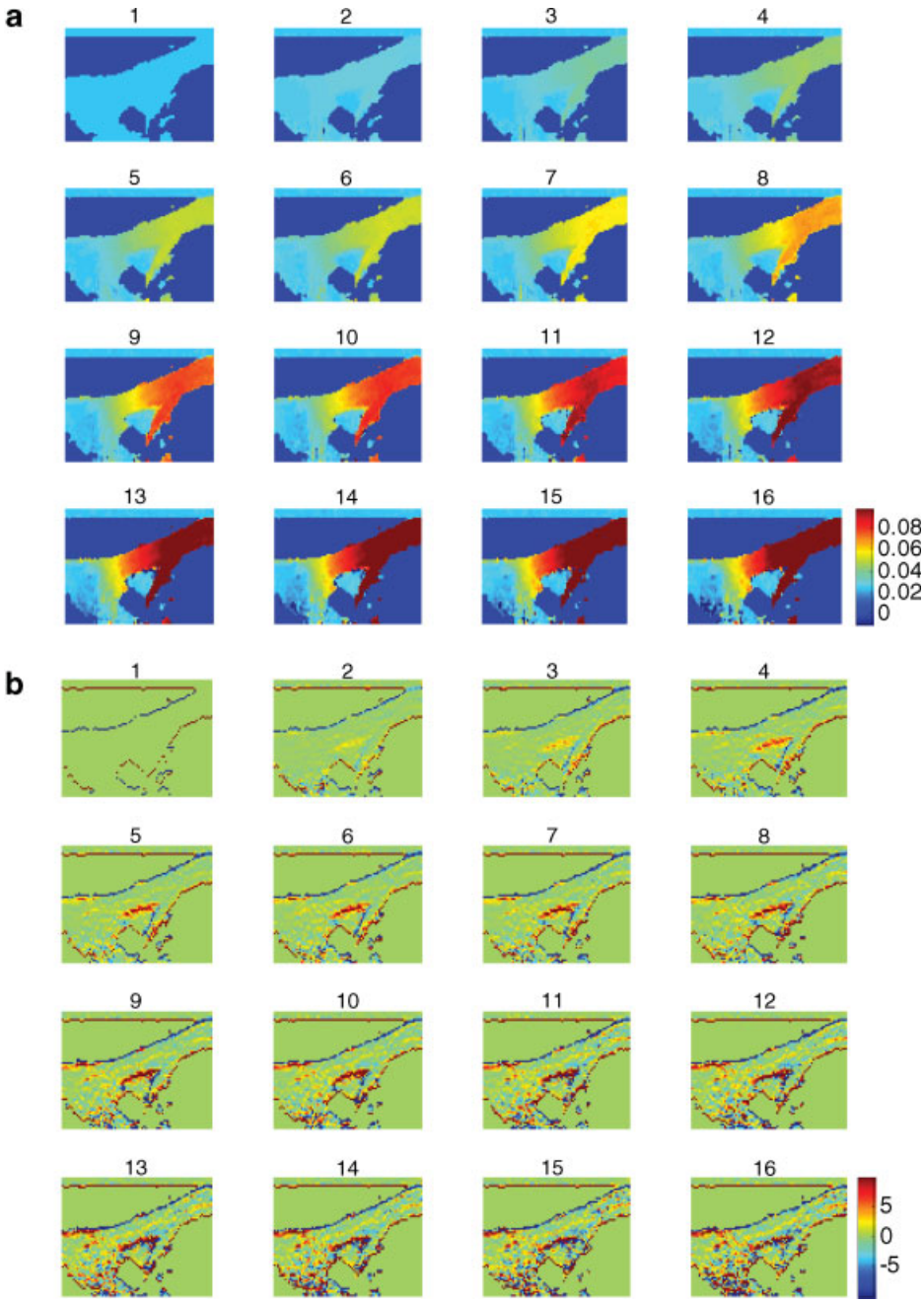

Figure 3. Sequential images of (a) axial displacement (mm) and (b) corresponding axial strain (%) elastograms during tensile loading of the femur-ACL-tibia complex. In the elastograms, blue denotes compressive stain and red represents tensile strain. Note the development of large displacement in the ligament compared to bone during applied loading (0.1 mm total displacement over 0.3 sec), as indicated by the change from blue to red in the ligament proper in (a).

dimensional limitations of traditional mechanical testing techniques and the subsurface nature of interfacial tissue motivate the need for novel analytical methodologies to evaluate insertion mechanical properties. Our results demonstrate that ultrasound elastography is a promising tool for determining the mechanical behavior of the ACL and its insertions. Ultrasound elastography as an elasticity imaging modality has been extensively validated theoretically and experimentally.[38–45,53] Several of the elastographic studies and related theoretical models focused on articular cartilage.[42,44,45] For example, poroelastography,[44] or elastographic imaging of poroelastic tissues, has

 DOI 10.1002/jor

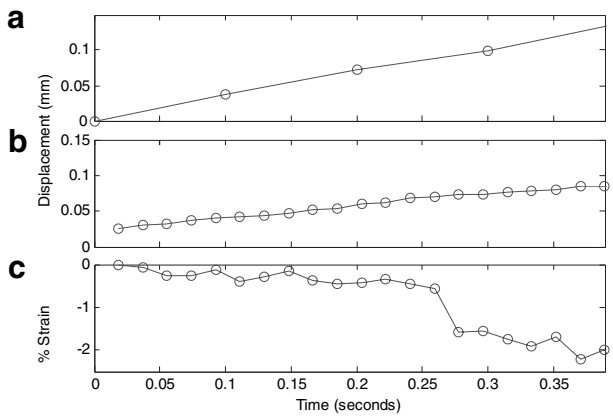

Figure 4. Comparison of pointwise elastographic analysis results with acquired tensile testing data. (a) Displacement in the femur–ACL–tibia complex as recorded by the MTS, with (b) corresponding variation in displacement and (c) corresponding strain at the tibial insertion calculated from pointwise temporal analysis of elastographic data. The selected point of data analysis corresponds to the region indicated by the arrow in Figure 2c and these results confirm the presence of compressive strain at the insertion site under applied tensile loading.

been used to estimate and image the in-plane strain ratio of simulated cartilage during sustained compression. Several groups have implemented traditional B-mode diagnostic ultrasound imaging for in vivo evalutation of ligamentous tissues.[46,54–61] Suzuki et al.[60] applied ultrasound imaging as a noninvasive tool for diagnosing injuries to the ACL, and Scherer et al.[58] used ultrasound to monitor postsurgery recovery of patients who had undergone ACL reconstruction. Recently, Revell et al.[62] utilized a block-matching technique to determine strain fields from dynamic sequences of ultrasound images of digital flexor and patellar tendons. Although these results demonstrate the applicability of this method for characterizing soft tissues, the block-matching method compares only ultrasound B-mode images, which limits the resolution and accuracy of the strain map as opposed to the RF data used in elastography.[38,44] In the present study, we have introduced the means for analyzing strain distribution in soft tissues and their insertions into bone with high accuracy and resolution.

Strain elastograms revealed that both tensile and compressive strain components were evident at the insertion site. Displacement was nonuniform throughout the femur–ACL–tibia complex, and strains experienced at the ACL insertions were highly complex. Although artifact negative strain values were first present in the ACL proper due to one-dimensional strain analysis, altering the transducer orientation confirmed that the strain in the ACL was predominantly tensile, while the strain distribution at the insertions was both tensile and compressive. Displacement images also revealed that deformation was higher in the ACL midsubstance compared to the tibial insertion, and that a gradual transition existed in the degree of deformation progressing from the ligament proper, through the tibial insertion, and finally into bone. These results suggest a tissue-dependent increase in stiffness from ligament to interface and then to bone, and confirms previous results from our laboratory, in which the compressive mechanical properties of the ACL–bone insertion sites were measured.[18]

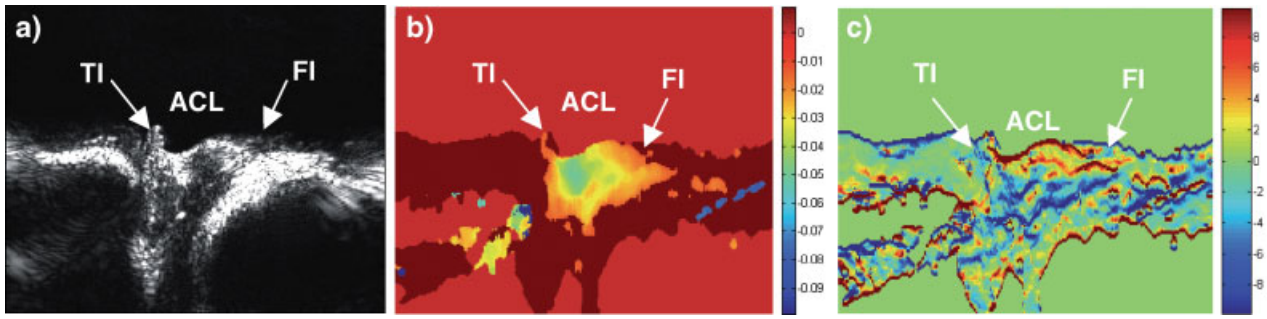

Figure 5. Effects of transducer orientation on elastographic analysis results. (a) Ultrasound image of ACL, femoral insertion (FI), and tibial insertion (TI) acquired with the face of the transducer aligned with the principal axis of the ACL. (b) Corresponding displacement map calculated from RF data, with red to blue indicating small-to-large displacements (mm), respectively. (c) Corresponding elastogram with percent compressive strain indicated in blue and tensile strain in red. Negative values denote compressive strain. Note that only tensile strain (red) was found at the ACL proper and compressive (blue) strain was again detected at the ACL–bone insertions (TI and FI).

Our results constitute the first experimental determination of the complex strain distribution at the insertion sites. Prior to this study, strain distribution at the soft tissue-bone interface had been predicted largely through FE analysis, as traditional mechanical testing techniques are unable to resolve subsurface strain on such a small length scale (the width of the interface is 780 ± 3 μm for neonatal bovine[63]). Our experimental findings corroborate those of FE analyses performed by Matyas et al.,[64] who predicted that when the medial collateral ligament (MCL) is loaded in tension, the principal stress component found at the femoral insertion is compressive. Although the angle of insertion differs between the MCL and ACL, fibrocartilage tissue is the dominant tissue type found at the bony insertion for both ligaments. The presence of fibrocartilage supports our finding that a compressive strain component exists at the interface, as fibrocartilaginous tissues are often found in regions of compression.[65,66] The complexity of strain distribution within the insertions may facilitate the transfer of tensile strain from the ligament to bone through this interfacial fibrocartilage tissue.[37] In addition, collagen fibers extending from ligament into bone at the insertions may transmit tensile, shear and compressive stresses through the fibrocartilage zones.[8]

Our findings and the developed methods will be used in future studies to elucidate the structure–function relationship at the ligament–bone interface. Our long-term goal is to translate this understanding to the design of biomimetic scaffold systems able to facilitate biological fixation of soft tissue grafts to bone. The intent of this study was to develop novel methods that will enable the experiemental analysis of ligament insertion strains; thus, the femur–ACL–tibia complex was only tested under uniaxial tension in a saline environment. Future studies will extend these methods to the evaluation of insertion mechanical properties under physiological loading in an anatomic orientation. Understanding the mechanical responses of the native ACL and its insertions are important in the evaluation of replacement graft healing. Ultrasound elastography may be used to determine the in situ distribution of strain at the ACL–bone insertions and graft–bone fixation sites in the clinical setting. This technique provides functional information regarding the ACL, and can image the degree of graft healing following ACL reconstruction. The methodology developed in this study may enable quantitative and noninvasive evaluation of the structural properties of the ligament as well as the healing graft, in turn providing a reliable method to predict clinical outcomes and devise optimal physical therapy regimens.

In summary, when the femur–ACL–tibia complex was loaded in tension, an increase in stiffness from ligament to bone was found, and strain distribution within the tibial ACL insertion included both compressive and tensile components. These findings corroborate reported FE predictions and provide experimental validation of previous assumptions regarding the mechanical response of the fibrocartilaginous interface at ligament-to-bone insertions. Results of this study augment our understanding of the insertion site, and will guide our efforts to regenerate a functional tendon–bone interface. Ongoing studies focus on the use of higher frequency ultrasound scanners to quantify the mechanical properties of the ACL insertions in vitro and translation of this technique to in situ analysis of both the ACL and reconstruction grafts.

ACKNOWLEDGMENTS

The authors thank Thomas Gardner of the Department of Orthopaedic Surgery at Columbia University for his assistance with the mechanical testing system, as well as Kristen Moffat and Hsin Sheila Chin of the Biomaterials and Interface Tissue Engineering Laboratory at Columbia University for their assistance with joint preparation and tensile testing. This study was supported by NIH/NIAMS (R21 AR052402-01A1, HHL), NSF Graduate Fellowship (GK-12 033 8329, JPS) and startup funds (HHL and EEK) from Columbia University.

REFERENCES

1. Brown CH Jr, Carson EW. 1999. Revision anterior cruciate ligament surgery. Clin Sports Med 18:109–171.
2. Johnson RJ. 1982. The anterior cruciate: a dilemma in sports medicine. Int J Sports Med 3:71–79.
3. United States Department of Health and Human Services , Centers for Disease Control and Prevention, National Center for Health Statistics. National Hospital Discharge Survey; 1996.
4. United States Department of Health and Human Services, Centers for Disease Control and Prevention, National Center for Health Statistics. National Survey of Ambulatory Surgery; 1996.
5. Bray RC, Leonard CA, Salo PT. 2002. Vascular physiology and long-term healing of partial ligament tears. J Orthop Res 20:984–989.
6. Barrett GR, Noojin FK, Hartzog CW, et al. 2002. Reconstruction of the anterior cruciate ligament in females: a comparison of hamstring versus patellar tendon autograft. Arthroscopy 18:46–54.

7. Beynnon BD, Johnson RJ, Fleming BC, et al. 2002. Anterior cruciate ligament replacement: comparison of bone–patellar tendon–bone grafts with two-strand hamstring grafts. A prospective, randomized study. J Bone Joint Surg Am 84-A:1503–1513.
8. Woo SL, Buckwalter JA. 1988. AAOS/NIH/ORS workshop. Injury and repair of the musculoskeletal soft tissues. Savannah, Georgia, June 18–20, 1987. J Orthop Res 6:907–931.
9. Wei X, Messner K. 1996. The postnatal development of the insertions of the medial collateral ligament in the rat knee. Anat Embryol (Berl) 193:53–59.
10. Woo SL, Gomez MA, Seguchi Y, et al. 1983. Measurement of mechanical properties of ligament substance from a bone–ligament–bone preparation. J Orthop Res 1: 22–29.
11. Friedman MJ, Sherman OH, Fox JM, et al. 1985. Autogeneic anterior cruciate ligament (ACL) anterior reconstruction of the knee. A review. Clin Orthop Relat Res 196:9–14.
12. Jackson DW, Grood ES, Arnoczky SP, et al. 1987. Cruciate reconstruction using freeze dried anterior cruciate ligament allograft and a ligament augmentation device (LAD). An experimental study in a goat model. Am J Sports Med 15:528–538.
13. Kurosaka M, Yoshiya S, Andrish JT. 1987. A biomechanical comparison of different surgical techniques of graft fixation in anterior cruciate ligament reconstruction. Am J Sports Med 15:225–229.
14. Robertson DB, Daniel DM, Biden E. 1986. Soft tissue fixation to bone. Am J Sports Med 14:398–403.
15. Rodeo SA, Suzuki K, Deng XH, et al. 1999. Use of recombinant human bone morphogenetic protein-2 to enhance tendon healing in a bone tunnel. Am J Sports Med 27:476–488.
16. Yahia L. Ligaments and ligamentoplasties. Berlin: Springer Verlag; 1997.
17. Lu HH, Jiang J. 2004. Interface tissue engineering and the formulation of multiple-tissue systems. In: Lee K, Kaplan DL, editors. Advances in biochemical engineering/biotechnology. New York: Springer Verlag.
18. Moffat KL, Chahine NO, Hung CT, et al. 2005. Characterization of the mechanical properties of the ACL-Bone insertion. Proceedings of the 2005 Bioengineering Conference (ASME) Bed 54:1–67.
19. Spalazzi JP, Costa KD, Doty SB, et al. 2004. Characterization of the mechanical properties, structure, and composition of the anterior cruciate ligament–bone insertion site. Trans Orthop Res Soc 29:1271.
20. Spalazzi JP, Doty SB, Moffat KL, et al. 2006. Development of controlled matrix heterogeneity on a triphasic scaffold for orthopedic interface tissue engineering. Tissue Eng, in press.
21. Butler DL, Guan Y, Kay MD, et al. 1992. Location-dependent variations in the material properties of the anterior cruciate ligament. J Biomech 25:511–518.
22. Butler DL, Martin ET, Kaiser AD, et al. 1988. The effects of flexion and tibial rotation on the 3-D orientations and lengths of human anterior cruciate ligament bundles. Trans Orthop Res Soc.
23. Butler DL, Sheh MY, Stouffer DC, et al. 1990. Surface strain variation in human patellar tendon and knee cruciate ligaments. J Biomech Eng 112:38–45.
24. Butler DL, Stouffer DC. 1983. Tension–torsion characteristics of the canine anterior cruciate ligament—Part II: experimental observations. J Biomech Eng 105:160–165.
25. Danto MI, Woo SL. 1993. The mechanical properties of skeletally mature rabbit anterior cruciate ligament and patellar tendon over a range of strain rates. J Orthop Res 11:58–67.
26. Figgie HE III, Bahniuk EH, Heiple KG, et al. 1986. The effects of tibial–femoral angle on the failure mechanics of the canine anterior cruciate ligament. J Biomech 19: 89–91.
27. Kwan MK, Lin TH, Woo SL. 1993. On the viscoelastic properties of the anteromedial bundle of the anterior cruciate ligament. J Biomech 26:447–452.
28. Trent PS, Walker PS, Wolf B. 1976. Ligament length patterns, strength, and rotational axes of the knee joint. Clin Orthop Relat Res 17:263–270.
29. Woo SL, Hollis JM, Adams DJ, et al. 1991. Tensile properties of the human femur–anterior cruciate ligament–tibia complex. The effects of specimen age and orientation. Am J Sports Med 19:217–225.
30. Woo SL, Newton PO, MacKenna DA, et al. 1992. A comparative evaluation of the mechanical properties of the rabbit medial collateral and anterior cruciate ligaments. J Biomech 25:377–386.
31. Yahia LH, Drouin G. 1990. Study of the hysteresis phenomenon in canine anterior cruciate ligaments. J Biomed Eng 12:57–62.
32. Hirokawa S, Tsuruno R. 2000. Three-dimensional deformation and stress distribution in an analytical/computational model of the anterior cruciate ligament. J Biomech 33:1069–1077.
33. Hirokawa S, Tsuruno R. 1997. Hyper-elastic model analysis of anterior cruciate ligament. Med Eng Phys 19: 637–651.
34. Limbert G, Middleton J, Taylor M. 2004. Finite element analysis of the human ACL subjected to passive anterior tibial loads. Comput Methods Biomech Biomed Eng 7: 1–8.
35. Limbert G, Taylor M, Middleton J. 2004. Three-dimensional finite element modelling of the human ACL: simulation of passive knee flexion with a stressed and stress-free ACL. J Biomech 37:1723–1731.
36. Song Y, Debski RE, Musahl V, et al. 2004. A three-dimensional finite element model of the human anterior cruciate ligament: a computational analysis with experimental validation. J Biomech 37:383–390.
37. Lerner RM, Huang SR, Parker KJ. 1990. "Sonoelasticity" images derived from ultrasound signals in mechanically vibrated tissues. Ultrasound Med Biol 16:231–239.
38. Ophir J, Cespedes I, Ponnekanti H, et al. 1991. Elastography: a quantitative method for imaging the elasticity of biological tissues. Ultrasound Imaging 13:111–134.
39. de Korte CL, Sierevogel MJ, Mastik F, et al. 2002. Identification of atherosclerotic plaque components with intravascular ultrasound elastography in vivo: a Yucatan pig study. Circulation 105:1627–1630.
40. Konofagou EE, D'hooge J, Ophir J. 2002. Myocardial elastography—a feasibility study in vivo. Ultrasound Med Biol 28:475–482.
41. Varghese T, Zagzebski JA, Lee FT Jr. 2002. Elastographic imaging of thermal lesions in the liver in vivo following radiofrequency ablation: preliminary results. Ultrasound Med Biol 28:1467–1473.
42. Brommer H, Brama PA, Laasanen MS, et al. 2005. Functional adaptation of articular cartilage from birth to

maturity under the influence of loading: a biomechanical analysis. Equine Vet J 37:148–154.
43. Fortin M, Buschmann MD, Bertrand MJ, et al. 2003. Dynamic measurement of internal solid displacement in articular cartilage using ultrasound backscatter. J Biomech 36:443–447.
44. Konofagou EE, Harrigan TP, Ophir J, et al. 2001. Poroelastography: imaging the poroelastic properties of tissues. Ultrasound Med Biol 27:1387–1397.
45. Zheng YP, Bridal SL, Shi J, et al. 2004. High resolution ultrasound elastomicroscopy imaging of soft tissues: system development and feasibility. Phys Med Biol 49: 3925–3938.
46. Schwarz W, Hagelstein J, Minholz R, et al. 1997. Manual ultrasound of the knee joint. A general practice method for diagnosis of fresh rupture of the anterior cruciate ligament. Unfallchirurg 100:280–285.
47. Abramowitch SD, Papageorgiou CD, Withrow JD, et al. 2003. The effect of initial graft tension on the biomechanical properties of a healing ACL replacement graft: a study in goats. J Orthop Res 21:708–715.
48. Musahl V, Abramowitch SD, Gabriel MT, et al. 2003. Tensile properties of an anterior cruciate ligament graft after bone–patellar tendon–bone press-fit fixation. Knee Surg Sports Traumatol Arthrosc 11:68–74.
49. Woo SL, Hollis JM, Roux RD, et al. 1987. Effects of knee flexion on the structural properties of the rabbit femur–anterior cruciate ligament–tibia complex (FATC). J Biomech 20:557–563.
50. Kallel F, Ophir J. 1997. A least-squares strain estimator for elastography. Ultrason Imaging 19:195–208.
51. Konofagou EE, Spalazzi JP, Lu HH. 2005. Elastographic imaging of strain distribution at the anterior cruciate ligament and ACL-bone insertions. IEEE-EMBS Proc 972–975
52. Spalazzi JP, Konofagou EE, Gallina J, et al. 2005. Elastographic imaging of strain distribution within the anterior cruciate ligament and at the ACL–bone insertions. IEEE-UFFC Proc 3:1755–1758.
53. Konofagou EE, Ophir J. 2000. Precision estimation and imaging of normal and shear components of the 3D strain tensor in elastography. Phys Med Biol 45:1553–1563.
54. Chylarecki C, Hierholzer G, Klose R. 1996. Ultrasound diagnosis of acute rupture of the anterior cruciate ligament. An experimental and clinical study. Unfallchirurg 99:24–30.
55. Fuchs S, Chylarecki C. 2002. Sonographic evaluation of ACL rupture signs compared to arthroscopic findings in acutely injured knees. Ultrasound Med Biol 28:149–154.
56. Jensen DB, Fischer-Rasmussen T, Magnusson SP, et al. 1999. Sonographic guided insertion of electrodes into the cruciate ligaments of the knee. Eur J Ultrasound 10: 47–51.
57. Richter J, David A, Pape HG, et al. 1996. Diagnosis of acute rupture of the anterior cruciate ligament. Value of ultrasonic in addition to clinical examination. Unfallchirurg 99:124–129.
58. Scherer MA, Kraus M, Gerngross H, et al. 1993. Importance of ultrasound in postoperative follow-up after reconstruction of the anterior cruciate ligament. Unfallchirurg 96:47–54.
59. Skovgaard Larsen LP, Rasmussen OS. 2000. Diagnosis of acute rupture of the anterior cruciate ligament of the knee by sonography. Eur J Ultrasound 12:163–167.
60. Suzuki S, Kasahara K, Futami T, et al. 1991. Ultrasound diagnosis of pathology of the anterior and posterior cruciate ligaments of the knee joint. Arch Orthop Trauma Surg 110:200–203.
61. Wittner B, Muller-Farber J. 1991. Value of sonography of the anterior cruciate ligament in post-traumatic hemarthrosis. Unfallchirurg 94:565–569.
62. Revell JD, Mirmehdi M, McNally DS. 2004. Musculoskeletal motion flow fields using hierarchical variable-sized block matching in ultrasonographic video sequences. J Biomech 37:511–522.
63. Wang IE, Mitroo S, Chen FH, et al. 2006. Age-dependent changes in matrix composition and organization at the ligament-to-bone insertion. J Orthop Res 24:1745–1755.
64. Matyas JR, Anton MG, Shrive NG, et al. 1995. Stress governs tissue phenotype at the femoral insertion of the rabbit MCL. J Biomech 28:147–157.
65. Benjamin M, Ralphs JR. 1998. Fibrocartilage in tendons and ligaments—an adaptation to compressive load. J Anat 193(Pt 4):481–494.
66. Evanko SP, Vogel KG. 1990. Ultrastructure and proteoglycan composition in the developing fibrocartilaginous region of bovine tendon. Matrix 10:420–436.

 DOI 10.1002/jor